Electronic Supplementary Material (ESI) for Dalton Transactions.

Spin-state versatility in $Fe^{II}_4L_6$ supramolecular cages with pyridyl-hydrazone ligand scaffold modulated by solvents and counter anions

Weiyang Li,[a] Xiaochun Li,[a] Koen Robeyns,[a] Mariusz Wolff,[b] Joseph Kfoury,[c] Julianna Oláh,[c] Radovan Herchel,[d] Serhiy Demeshko,[e] Franc Meyer,[e] Yann Garcia*[a]

[a] Institute of Condensed Matter and Nanosciences, Molecular Chemistry, Materials and Catalysis (IMC/MOST), Université catholique de Louvain, Place Louis Pasteur 1, 1348 Louvain-la-Neuve, Belgium

[b] Institut für Chemische Katalyse, Fakultät für Chemie, Universität Wien, Währinger Strasse 38, 1090 Wien, Austria

[c] Department of Inorganic and Analytical Chemistry, Budapest University of Technology and Economics, H-1111 Szent Gellért tér 4, Budapest, Hungary

[d] Department of Inorganic Chemistry, Faculty of Science, Palacký University, 17. Listopadu 12, 77146 Olomouc, Czech Republic

[e] Institut für Anorganische Chemie, Universität Göttingen, Tammannstrasse 4, D-37077 Göttingen, Germany

General information

All chemicals were purchased from commercial sources and used as supplied. $Fe(ClO_4)_2 \cdot 6H_2O$ and $Fe(CF_3SO_3)_2$ were purchased from Sigma-Aldrich and fluorochem, respectively. Elemental analyses (C, H, and N) were performed on Thermo Scientific Flash 2000 Analyzer. Thermogravimetric analyses (TGAs) were operated in $N_{2(g)}$ at a heating rate of 2 $^oC\ min^{-1}$ (10 $^oC\ min^{-1}$) from 25 ^oC to 200 ^oC (25 ^oC to 850 ^oC) with Mettler Toledo TGA/SDTA 851e analyzer for **2** (**3**). Electrospray ionization time-of-flight mass spectra (ESI-TOF-MS) were recorded on a Bruker maXis UHR ESI-Qq-TOF mass spectrometer in the positive ion mode. Scanning electron microscopy with energy-dispersive X-ray spectroscopy (SEM-EDS) were measured on JEOL 7600F. Fourier-Transform Infrared (FT-IR) spectra were collected on Equinox 55 (Bruker) equipped with an ATR modulus and an MCT detector. Diffuse reflectance spectra were collected on PerkinElmer Lambda 9 UV/vis/NIR spectrophotometer with a 60 mm integrating sphere and converted into absorption spectra by Kubelka−Munk function. $BaSO_4$ was used as a reference. Magnetic susceptibility for the cage family was measured on a Quantum Design MPMS3 SQUID magnetometer under an applied field of 5000 Oe. Magnetic data were corrected for the sample holder and diamagnetic contributions. ^{57}Fe Mössbauer spectra were recorded with a ^{57}Co source embedded in a Rh matrix using an alternating constant acceleration Wissel Mössbauer spectrometer operated in the transmission mode and equipped with a Janis closed-cycle helium cryostat. The spectra were fitted with the Mfit program and isomer shift values are given with respect to α-Fe at room temperature.

Mfit program：E. Bill, Max-Planck Institute for Chemical Energy Conversion, Mülheim/Ruhr, Germany

Table S1 Fe-Fe distance, cavity volume and anions position of all reported Fe^{II} SCO cages.

Cage	Temperature (K)	Fe-Fe $distance_{av}$ (Å)	Cavity volume ($Å^3$)	Anions inside/outside cavity	CCDC number
$[Fe_4L1_4](BF_4)_8 \cdot 14.75MeCN \cdot 4.5C_6H_6 \cdot 3H_2O$	153	14.16	108.84	inside	907705
$[Fe_4L1_4](BF_4)_8 \cdot 14.75MeCN \cdot 4.5C_6H_6 \cdot 3H_2O$	293	14.33	112.30	inside	907706
$[Fe_4L3_4](CF_3SO_3)_8$	100	11.85	57.05	outside	908546
$[Fe_4L4_4](BF_4)_4 \cdot 16CH_3CN$	100	14.76	202.09	outside	1057843
$[Fe4L5_6](BF_4)_8$+ [solvent]	100	12.75	78.13*	inside	1914986
$[Fe_4L6)_6](ClO_4)_8$ (R)	150	9.62	85.02	inside	1025013
$[Fe_4L6)_6](ClO_4)_8$ (S)	123	9.57	81.07	inside	1025014
$[Fe_4(L7)_6](ClO_4)_8 \cdot 11.59MeCN \cdot 2C_4H_{10}O \cdot H_2O$ (R)	123	9.64	85.42	inside	1025015
$[Fe_4(L7)_6](ClO_4)_8 \cdot 6MeCN$ (S)	123	9.68	89.73	inside	1025016
$[Fe_4(L8)_6](ClO_4)_8 \cdot 2MeCN$ (S)	123	9.67	90.46	inside	1025017
$[Fe_4(L9)_6](BF_4)_8$	173	11.38	1D channel	-	1447306
$[Fe_4(L10)_6](ClO_4)_8$	173	9.59	83.98	outside	1873319
$[Fe_4(L11)_6](CF_3SO_3)_8$+ [solvent]	173	12.38	cube-like cavities	-	1847958
$[Fe_4$ $(L12)_6](CF_3SO_3)_8$+ [solvent]	173	12.23	cube-like cavities	-	1847959
$[Fe_4(L13)_6](ClO_4)_8 \cdot 10MeNO_2 \cdot 5.6H_2O$	113	8.68	0	outside	1959705
$[Fe_4(L14)_6](BF_4)_8 \cdot 10.8MeCN \cdot 4H_2O$	113	8.73	0	outside	1959706
Cage 1	120	12.71	0	outside	2191810
Cage 2	120	12.63	0	outside	2270896
Cage 3	100	12.29	0	-	2270897

Cavity volumes were calculated by MoloVol (*J. Appl. Crystallogr.* **2022**, *55*, 1033-1044.)

*: Large probe radius in Å = 3; Spatial resolution of the underlying grid in Å = 0.5. The rest of calculations were done with default values of 1.2 Å and 0.2 Å, respectively.

'-': Indicates that either the tetrahedral cavity is not confined, or anions cannot be determined from the single crystal structure.

No significant cavity volume was observed with the MoloVol software for **1**-**3**. This is probably due to the rotation of the linear ligands located on the tetrahedral edges causing the phenyl ring to be guided into the cavity, thus reducing the volume in the cavity (*Chem. Commun.*, 2013, **49**, 1597-1599). In some way, this contrasts with the face-capped configuration cage.

Single-crystal X-ray diffraction analyses

The structural analyses for cage **2** (120 K) and **3** (100 K) were performed on MAR345 image plate using Mo-Kα radiation (λ = 0.71073Å), generated by an Incoatec IμS generator equipped with Montel Mirrors. Prior to data collection the crystals were flash frozen at corresponding low temperature. CrysAlis^{PRO} was used for data integration and reduction and the implemented absorption correction was applied. The crystals of cages **2** and **3** were quite small and unstable. Because diethyl ether was used as anti-solvent, crystals readily redissolved into the mother liquid (acetonitrile) when exposed to air and the diethyl ether evaporates. The structures of **2** were solved by SHELXT and showed one cage systems in the asymmetric unit along with the eight ClO_4^- counter anions, two of which were disordered and all located around the cage, with no anions found inside the cavity. Refinement was done by full-matrix least squares on F^2 using SHELXL2018/3. Although data were collected to 0.8 Å, a data cut-off of 1 Å was imposed during integration beyond which the crystal diffracted poorly. The structure of **3** showed two cage systems in the asymmetric unit, yet only thirteen OTf^- anions were found (excepted sixteen anions for eight Fe^{II} ions), the remaining (disordered) anions probably reside in the large solvent cavity (25% of the unit cell volume). The electron density inside this cavity was taken into account by the SQUEEZE procedure in PLATON. Final crystallographic data and refinement values for cages **2** and **3** are listed in Table 1. CCDC 2270896-2270897 contain the supplementary crystallographic data for this paper.

SHELXT:

Sheldrick, G. M. (2015). *Acta Cryst.* A**71**, 3-8.

Crysalis^{PRO}:

Rigaku (2015). *CrysAlisPro Software System*, Version 1.171.38.41. Rigaku Oxford Diffraction

PLATON SQUEEZE:

Spek, A. L. (2015). *Acta Cryst.* C**71**, 9-18.

Synthesis of cage **2**

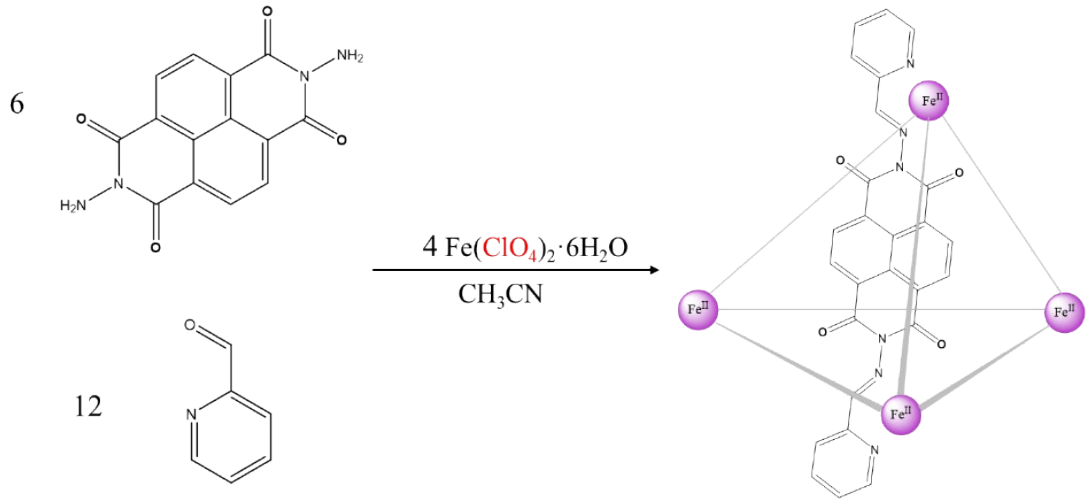

Schematic illustration of the construction of cage **2**.

N, *N*-diaminonaphthalene-1,4,5,8-tetracarboxydi-imide (37 mg, 0.125 mmol), $Fe(ClO_4)_2 \cdot 6H_2O$ (30 mg, 0.083 mmol), and 2-formylpyridine (24 μL, 0.25 mmol) were dissolved in acetonitrile (40 mL). The reaction mixture was stirred in a Schlenk flask under argon at 65 °C overnight. After cooling to room temperature, the resulting purple solution was filtered. Cage **2** was obtained as red single crystals through slow diffusion of diethyl ether into the filtrate at room temperature after one week. Yield: 27.4 mg (34%). Elemental analysis (%) for crystals rinsed with diethyl ether and dried. Calcd. for $C_{156}H_{84}O_{24}N_{36}Fe_4Cl_8O_{32} \cdot 10H_2O$, C,46.31%; H, 2.60%; N, 12.46%; found C, 46.23%; H, 2.70%; N, 12.15%. ESI-TOF-MS: *m/z* Calcd. for $[Fe_4L_6(ClO_4)_5]^{3+}$ 1189.0431, found 1189.0433; Calcd. for $[Fe_4L_6(ClO_4)_4]^{4+}$ 866.7953, found 866.7963; Calcd. for $[Fe_4L_6(ClO_4)_3]^{5+}$ 673.6465, found 673.6477; Calcd. for $[Fe_4L_6(ClO_4)]^{7+}$ 452.7622, found 452.7633; Calcd. for $[Fe_4L_6]^{8+}$ 383.6732, found 383.6741.

Synthesis of cage **3**

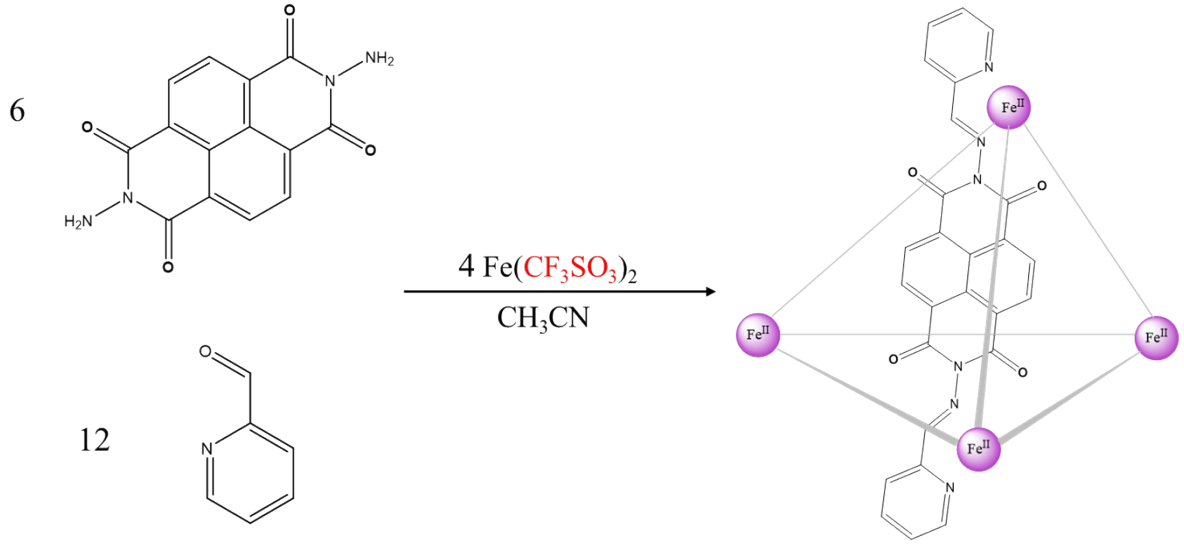

Schematic illustration of the construction of cage **3**.

N, *N*-diaminonaphthalene-1,4,5,8-tetracarboxydi-imide (37 mg, 0.125 mmol), $Fe(CF_3SO_3)_2$ (30 mg, 0.083 mmol), and 2-formylpyridine (24 μL, 0.25 mmol) were dissolved in acetonitrile (40 mL). The reaction mixture was stirred in a Schlenk flask under argon at 65 °C overnight. After cooling to room temperature, the resulting purple solution was filtered. Single crystals of cage **3** were obtained through slow diffusion of diethyl ether into the filtrate at room temperature after several days. Yield: 23.1 mg (26%). Elemental analysis (%) for crystals rinsed with diethyl ether and dried. Calcd. for $C_{164}H_{84}O_{48}N_{36}Fe_4F_{24}S_8 \cdot 13H_2O$, C,43.80%; H, 2.47%; N, 11.21%; found C, 43.74%; H, 2.33%; N, 11.03%. ESI-TOF-MS: *m/z* Calcd. for $[Fe_4L_6(CF_3SO_3)_5]^{3+}$ 1271.7165, found 1271.7168; Calcd. for $[Fe_4L_6(CF_3SO_3)_4]^{4+}$ 916.5493, found 916.5505; Calcd. for $[Fe_4L_6(CF_3SO_3)_3]^{5+}$ 703.2487, found 703.2502; Calcd. for $[Fe_4L_6(CF_3SO_3)]^{7+}$ 459.7626, found 459.7639; Calcd. for $[Fe_4L_6]^{8+}$ 383.6732, found 383.6742.

Table S2. Fe−N bond lengths (Å) for **2** at 120 K.

Fe (II) centers	Average Fe-N bond length (Å)	Spin-state
Fe(1)	1.96	LS
Fe(2)	1.98	LS
Fe(3)	1.98	LS
Fe(4)	1.99	LS

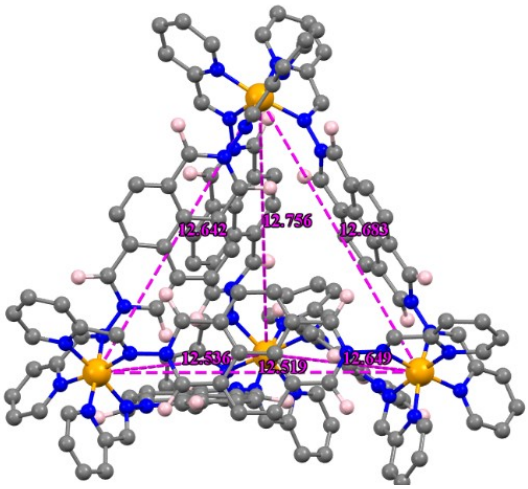

Fig. S1 Fe-Fe distance (Å) within the tetrahedron of **2**.

Table S3. Fe−N bond lengths (Å) for cage **3** at 100 K.

Fe (II) centers	Average Fe-N bond length (Å)	Spin-state
Fe(1)	1.98	LS
Fe(2)	1.97	LS
Fe(3)	2.00	LS
Fe(4)	2.00	LS

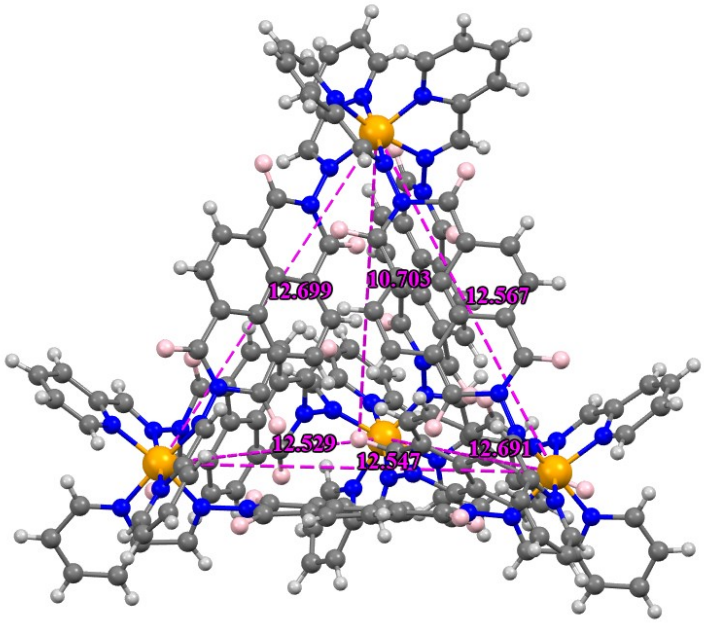

Fig. S2 Fe-Fe distance (Å) within the tetrahedron of **3**.

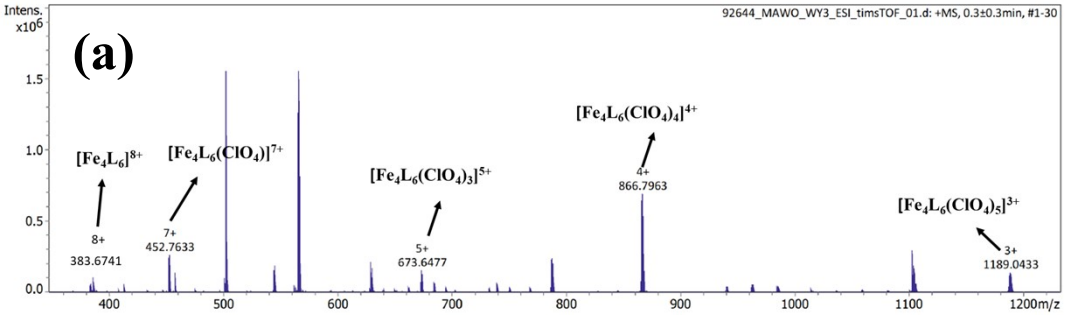

Fig. S3a ESI-TOF-MS spectrum of cage **2**.

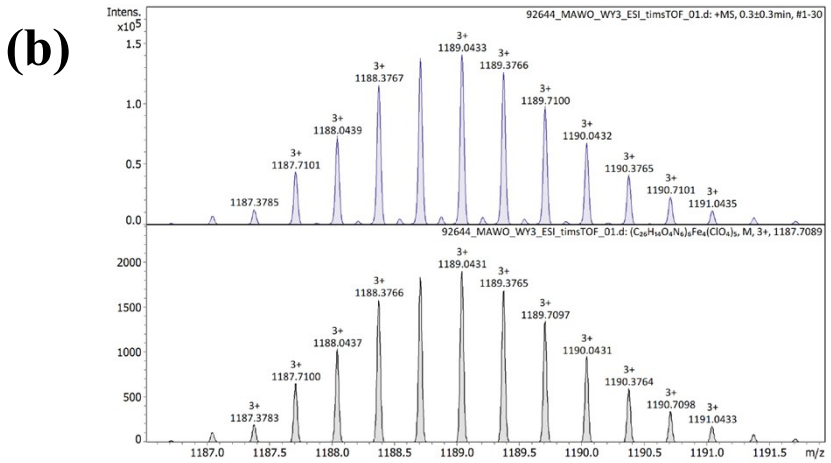

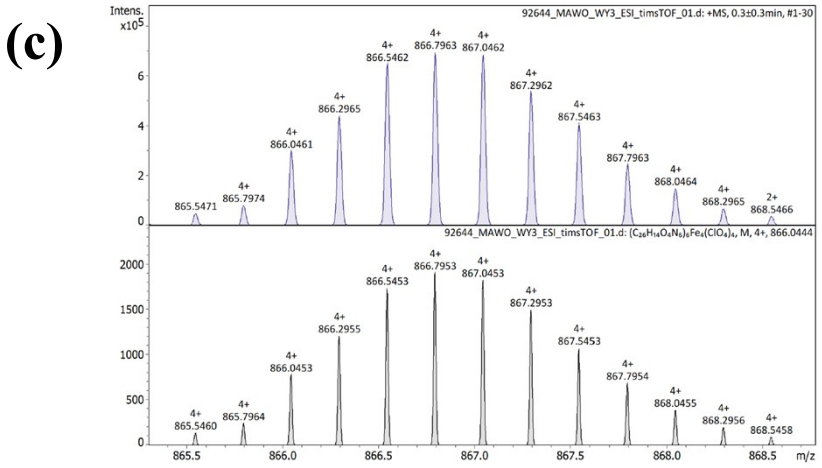

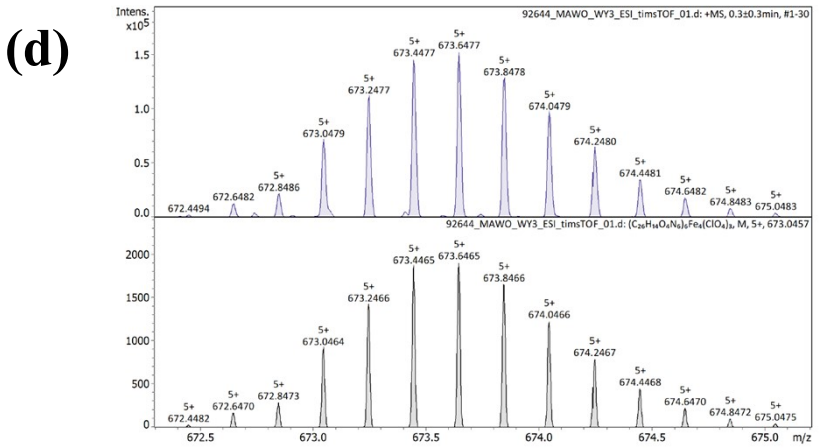

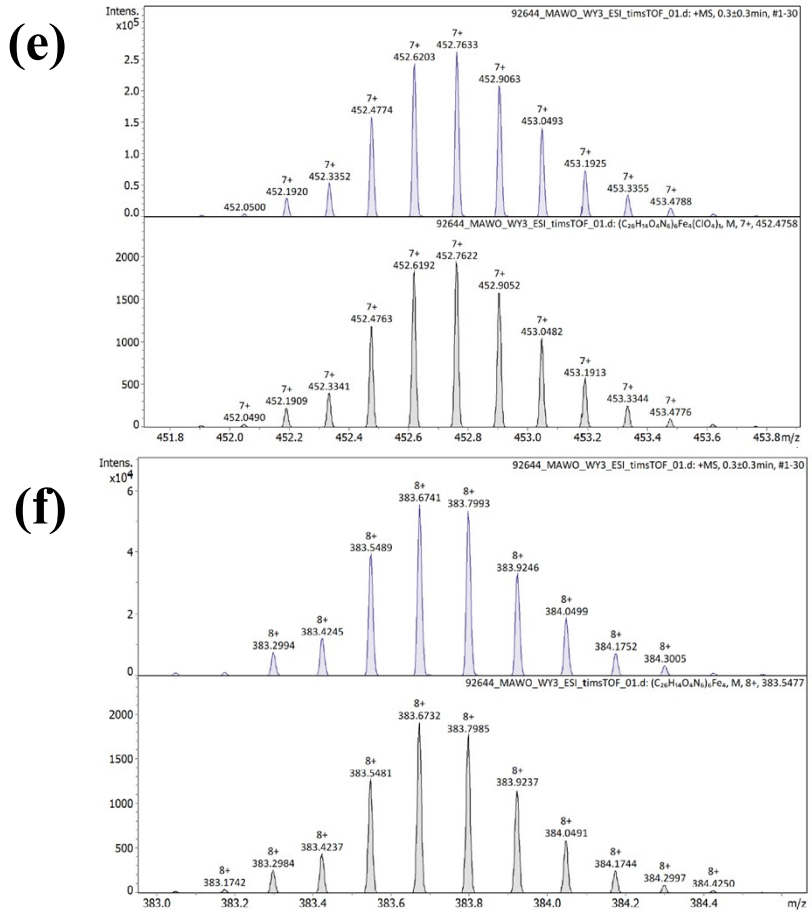

Fig. S3b-S3f Comparison of the observed isotopic patterns with the simulated spectra for different charge states from 3+ to 8+ of cage **2**.

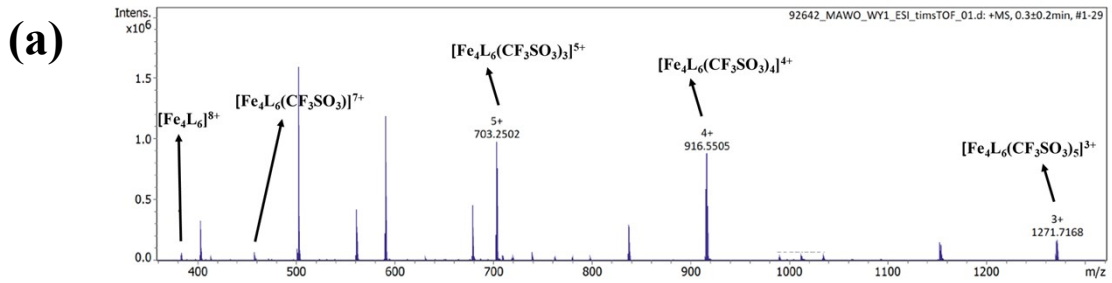

Fig. S4a ESI-TOF-MS spectrum of cage **3**.

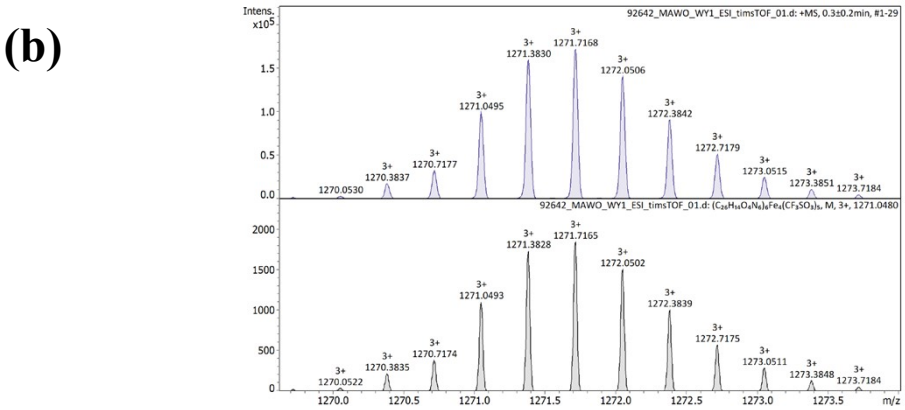

(c)

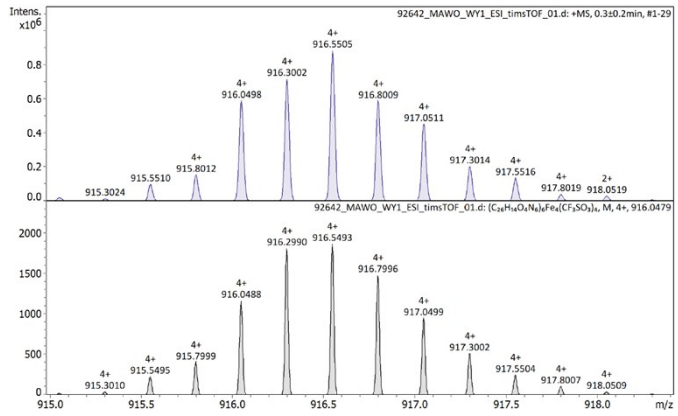

(d)

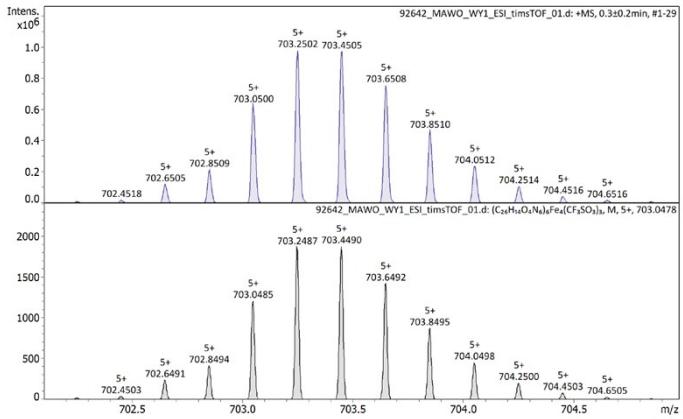

(e)

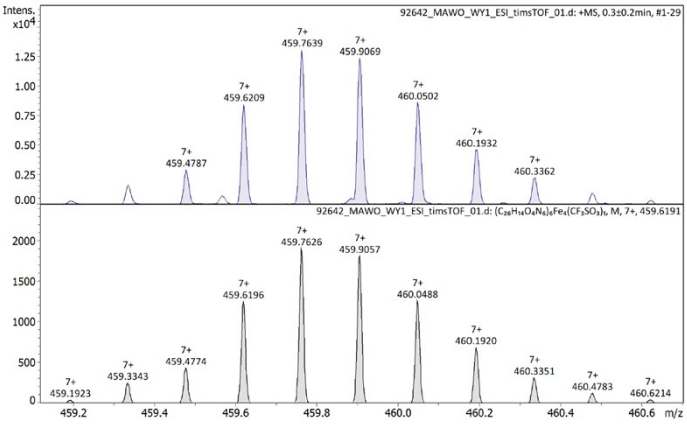

(f)

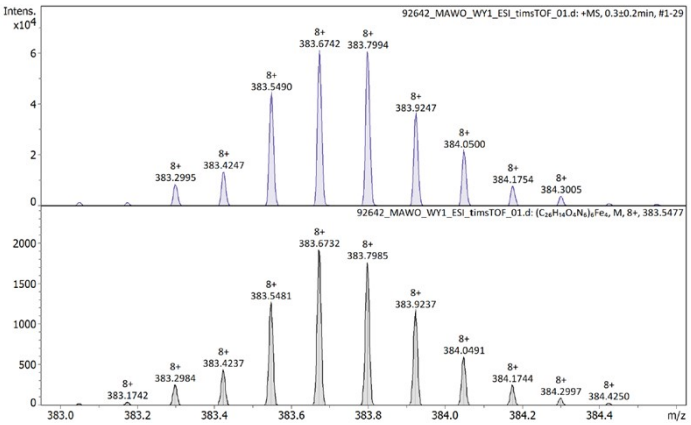

Fig. S4b-S4f Comparison of the observed isotopic patterns with the simulated spectra for different charge states from 3+ to 8+ of cage **3**.

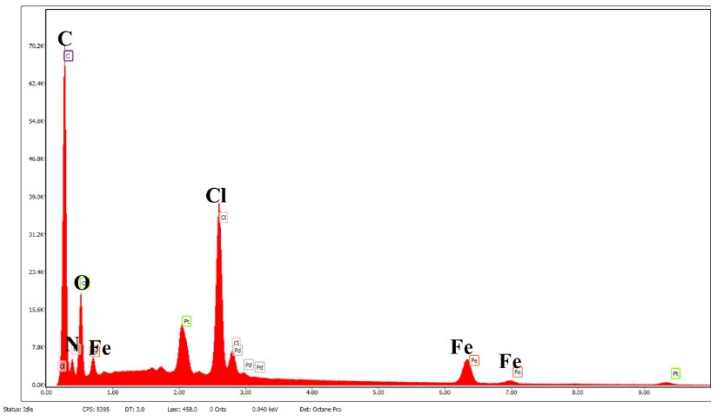

Fig. S5 EDS spectrum of **2**. Pt and Pd signals are from sample preparation.

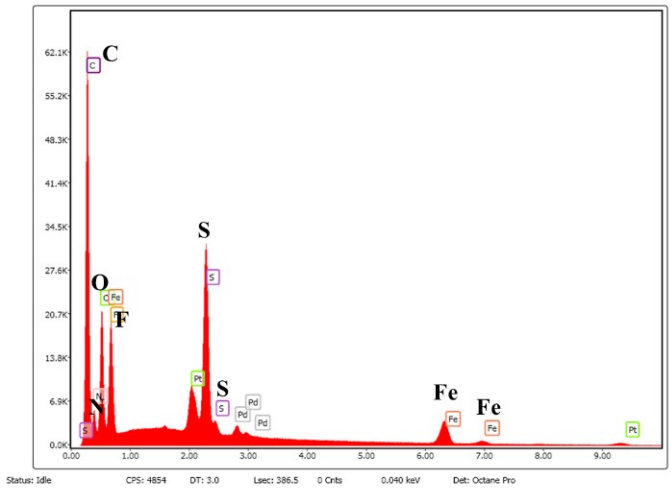

Fig. S6 EDS spectrum of **3**. Pt and Pd signals are from sample preparation.

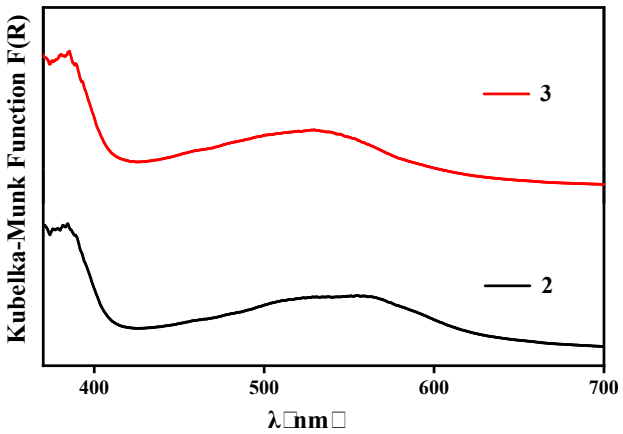

Fig. S7 Diffuse reflectance spectra of **2** and **3**.

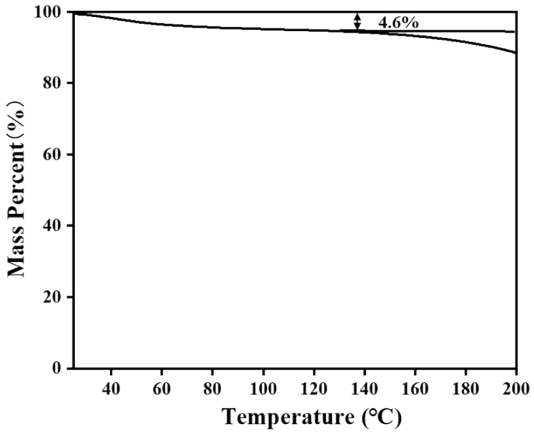

Fig. S8 TGA profile of **2**. The mass loss of *c.a.* 4.6% from room temperature to 130 °C, which is attributed to the release of 10 water molecules, matching well elemental analysis result (4.5%).

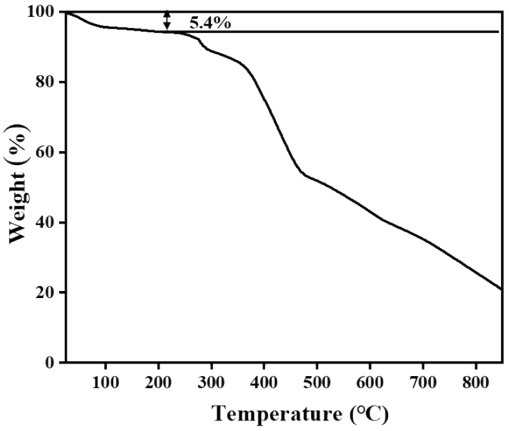

Fig. S9 TGA profile of **3**. The mass loss of *c.a.* 5.4% from room temperature to 200 °C, which is attributed to the release of 10 water molecules, matching well elemental analysis result (5.2%).

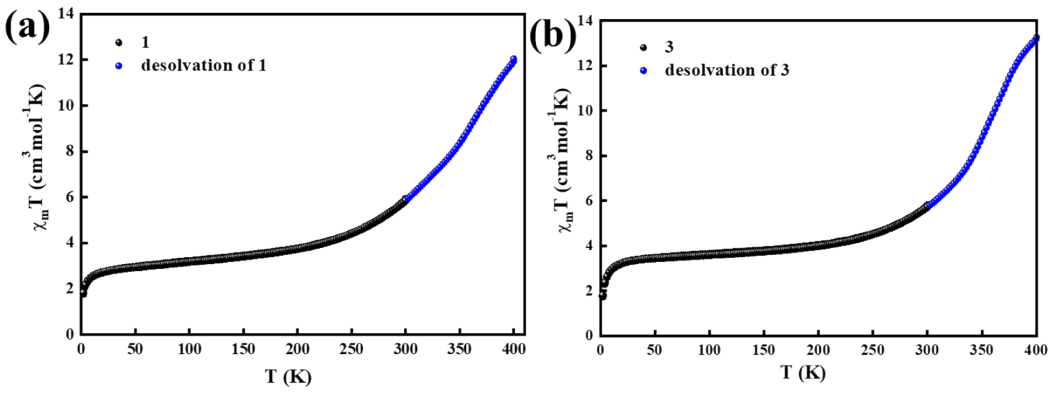

Fig. S10 Temperature dependence of the $\chi_m T$ product for **1** (a) and **3** (b) before desolvation (black circles; 300-2-300 K) and desolvation processes of **1** (a) and **3** (b) in the SQUID chamber (blue circles; 300-400 K).

Computational Details:

The ORCA 5.0.4 program was used for all calculations.[1,2] As the whole cages together with the anions were too large to be simulated, first we studied the cage without anions (+8 charge) with systematically changing the spin state of one iron centre at a time. This way the geometries of 4LS, 3LS-1HS, 2LS-2HS, 1LS-3HS, and 4HS spin isomers of $[Fe^{II}_4L_6]^{8+}$ cage complexes cations were optimized with BP86 functional using def2-TZVP for Fe atoms, def2-TZVP(-f) for N and O atoms, def2-SVP for C and H atoms – Table S4-S5. The calculations were sped up using the resolution of identity (RI) and def2/J auxiliary basis set. Additionally, the correction to dispersion energies D4 were also applied together with the CPCM solvation model (with water as solvent). For all calculations, tight convergence criteria (tightSCF and tightOPT) and highest numerical grid (defgrid3) were used.

Such procedure was also used for geometry optimization of mononuclear iron complexes for the calibration of the isomer shift for ^{57}Fe Mösssbauer spectroscopy – Table S7.

The single-point electronic energies were calculated with hybrid functional B3LYP and with hybrid meta-GGA functional TPSSh for all 4LS, 3LS-1HS, 2LS-2HS, 1LS-3HS, and 4HS spin isomers of $[Fe^{II}_4L_6]^{8+}$ cage complex (Table S6, Figure S11), and also for all mononuclear iron(II) complexes chosen for the calibration of the isomer shift for ^{57}Fe Mösssbauer spectroscopy. Herein, CP(PPP) basis set was used for Fe atoms and def2-TZVP for all other atoms. The calculations used the chain-of-spheres approximation to exact exchange (RIJCOSX)[1],[2] with the auxiliary basis def2/J and others created by an AutoAux generation procedure.[3] Again, the correction to dispersion energies D4 were also applied together with the CPCM solvation model (with water as solvent), and tight convergence criteria (tightSCF) and highest numerical grid (defgrid3) were used.

[1] R. Izsak, F. Neese, J. Chem. Phys. 135 (14) (2011) 144105
[2] F. Neese, F. Wennmohs, A. Hansen, U. Becker, Chem. Phys. 356 (2009) 98–109.
[3] G.L. Stoychev, A.A. Auer, F. Neese, J. Chem. Theory Comput. 13 (2017) 554–562.

Table S4. OctaDist analysis of coordination polyhedra in DFT calculated geometries of 4LS, 3LS-1HS, 2LS-2HS, 1LS-3HS, and 4HS spin isomers of $[Fe^{II}_4L_6]^{8+}$ cage complex.

4LS	Metal center	Spin State	$d(Fe\text{-}N)_{avg}$ (Å)	z	D	S	Q
	1	LS	1.964	0.0591	0.000042	59.02	195.44
	2	LS	1.964	0.0597	0.000042	59.78	196.60
	3	LS	1.964	0.0602	0.000044	59.43	196.13
	4	LS	1.965	0.0580	0.000042	59.46	196.15
3LS-1HS	Metal center	Spin State	$d(Fe\text{-}N)_{avg}$ (Å)	z	D	S	Q
	1	HS	2.158	0.0510	0.000018	88.58	273.01
	2	LS	1.964	0.0713	0.000062	60.20	196.08
	3	LS	1.964	0.0548	0.000038	59.83	195.78
	4	LS	1.964	0.0514	0.000033	59.03	195.69
2LS-2HS	Metal center	Spin State	$d(Fe\text{-}N)_{avg}$ (Å)	z	D	S	Q
	1	HS	2.158	0.0460	0.000017	88.34	270.87
	2	HS	2.158	0.0889	0.000052	89.65	281.15
	3	LS	1.963	0.0659	0.000058	60.30	195.30
	4	LS	1.964	0.0495	0.000030	59.29	195.17
1LS-3HS	Metal center	Spin State	$d(Fe\text{-}N)_{avg}$ (Å)	z	D	S	Q
	1	LS	1.963	0.0623	0.000052	59.72	194.29
	2	HS	2.156	0.0415	0.000014	87.14	269.25
	3	HS	2.158	0.0755	0.000035	89.30	274.09
	4	HS	2.156	0.0660	0.000029	88.94	275.74
4HS	Metal center	Spin State	$d(Fe\text{-}N)_{avg}$ (Å)	z	D	S	Q
	1	HS	2.156	0.0513	0.000017	88.57	273.71
	2	HS	2.156	0.0557	0.000021	88.26	274.29
	3	HS	2.156	0.0577	0.000021	88.28	272.09
	4	HS	2.156	0.0516	0.000017	88.08	272.26

The individual parameters are defined as:

$$\zeta = \sum_{i=1}^{6} |d_i - d_{mean}| \qquad \Delta = \frac{1}{6}\sum_{i=1}^{6}\left(\frac{d_i - d_{mean}}{d_{mean}}\right)^2 \qquad \Sigma = \sum_{i=1}^{12} |90 - \phi_i| \qquad \Theta = \sum_{i=1}^{24} |60 - \theta_i|$$

Table S5. Calculated volume of tetrahedron defined by the atomic positions of four Fe atoms in DFT calculated geometries of 4LS, 3LS-1HS, 2LS-2HS, 1LS-3HS, and 4HS spin isomers of $[Fe^{II}_4L_6]^{8+}$ cage complex.

	4LS	**3LS-1HS**	**2LS-2HS**	**1LS-3HS**	**4HS**
V (Å^3)	226.4	228.8	230.7	232.6	235.2
Relative change of volume for each step		1.05%	0.82%	0.83%	1.12%

Table S6. DFT calculated single-point energies for 4LS, 3LS-1HS, 2LS-2HS, 1LS-3HS, and 4HS spin isomers of $[Fe^{II}_4L_6]^{8+}$ cage complex.

BP86	**4LS**	**3LS-1HS**	**2LS-2HS**	**1LS-3HS**	**4HS**
Energy (E_h)	-14825.4461128	-14825.3927847	-14825.3393899	-14825.2854457	-14825.2312867
Relative energy (kcal/mol)	0.0	33.5	67.0	100.8	134.8
Relative change of energy (kcal/mol)		33.5	33.5	33.9	34.0
Mulliken atomic charges on Fe atoms	-0.728969 -0.729336 -0.729735 -0.726194	0.298299 -0.732281 -0.734167 -0.725470	0.297919 0.290505 -0.738334 -0.730956	-0.737577 0.291079 0.296583 0.293033	0.296296 0.290752 0.292673 0.292317
Mulliken spin populations on Fe atoms		3.808051 0.000017 0.000030 0.000034	3.807934 3.805776 0.000046 0.000066	0.000084 3.805342 3.805621 3.805503	3.805018 3.804439 3.804181 3.805050
Löwdin atomic charges on Fe atoms	-0.571574 -0.571565 -0.571217 -0.570852	-0.133650 -0.571952 -0.571571 -0.570939	-0.134030 -0.135167 -0.572261 -0.571317	-0.572502 -0.135972 -0.135047 -0.135932	-0.135422 -0.135979 -0.136747 -0.135836
Löwdin spin populations on Fe atoms		3.653662 0.000013 0.000024 0.000026	3.653712 3.651387 0.000036 0.000051	0.000065 3.650013 3.651536 3.650553	3.650049 3.649182 3.649023 3.649929
B3LYP	**4LS**	**3LS-1HS**	**2LS-2HS**	**1LS-3HS**	**4HS**
Energy (E_h)	-14824.8805129	-14824.8749827	-14824.8691233	-14824.8629728	-14824.8570781
Relative energy (kcal/mol)	0.0	3.5	7.1	11.0	14.7
Relative change of energy (kcal/mol)		3.5	3.7	3.9	3.7
Mulliken atomic charges on Fe atoms	0.149241 0.151474 0.150885 0.150464	0.797813 0.146558 0.148492 0.151288	0.797469 0.797497 0.143467 0.148455	0.141265 0.796803 0.795071 0.795098	0.793390 0.796181 0.795537 0.795272
Mulliken spin populations on Fe atoms		3.845192 0.000002 0.000004 0.000005	3.845231 3.845075 0.000006 0.000009	0.000011 3.843947 3.844628 3.844737	3.844196 3.843815 3.843822 3.844065
Löwdin atomic charges on Fe atoms	0.372925 0.372996 0.373244 0.373278	0.676526 0.373256 0.372988 0.373254	0.676775 0.676243 0.373178 0.373033	0.372865 0.675778 0.676368 0.675480	0.675573 0.675583 0.675175 0.675563
Löwdin spin populations on Fe atoms		3.723418 0.000001 0.000003 0.000004	3.723351 3.722712 0.000004 0.000008	0.000008 3.721443 3.722575 3.722169	3.721833 3.721327 3.721219 3.721634
TPSSh	**4LS**	**3LS-1HS**	**2LS-2HS**	**1LS-3HS**	**4HS**
Energy (E_h)	-14831.0706666	-14831.0429567	-14831.0149901	-14830.9863422	-14830.9577393
Relative energy (kcal/mol)	0.0	17.4	34.9	52.9	70.9
Relative change of energy (kcal/mol)		17.4	17.5	18.0	17.9
Mulliken atomic charges on Fe atoms	-0.013256 -0.011223 -0.011997 -0.010672	0.701382 -0.016034 -0.015501 -0.008432	0.703720 0.699583 -0.020336 -0.012318	-0.021641 0.701325 0.700228 0.694915	0.695166 0.698463 0.697314 0.697149
Mulliken spin populations on Fe atoms		3.873557 0.000004 0.000007 0.000009	3.873627 3.873602 0.000010 0.000017	0.000020 3.871932 3.872714 3.872902	3.872197 3.871815 3.871551 3.872014
Löwdin atomic charges on Fe atoms	0.386018 0.386064 0.386268 0.386360	0.683578 0.386323 0.386055 0.386371	0.683862 0.683291 0.386278 0.386186	0.386038 0.682944 0.683309 0.682524	0.682617 0.682684 0.682162 0.682693
Löwdin spin populations on Fe atoms		3.715918 0.000001 0.000007 0.000008	3.715877 3.715021 0.000008 0.000015	0.000016 3.713379 3.714781 3.714276	3.713798 3.713174 3.713020 3.713602

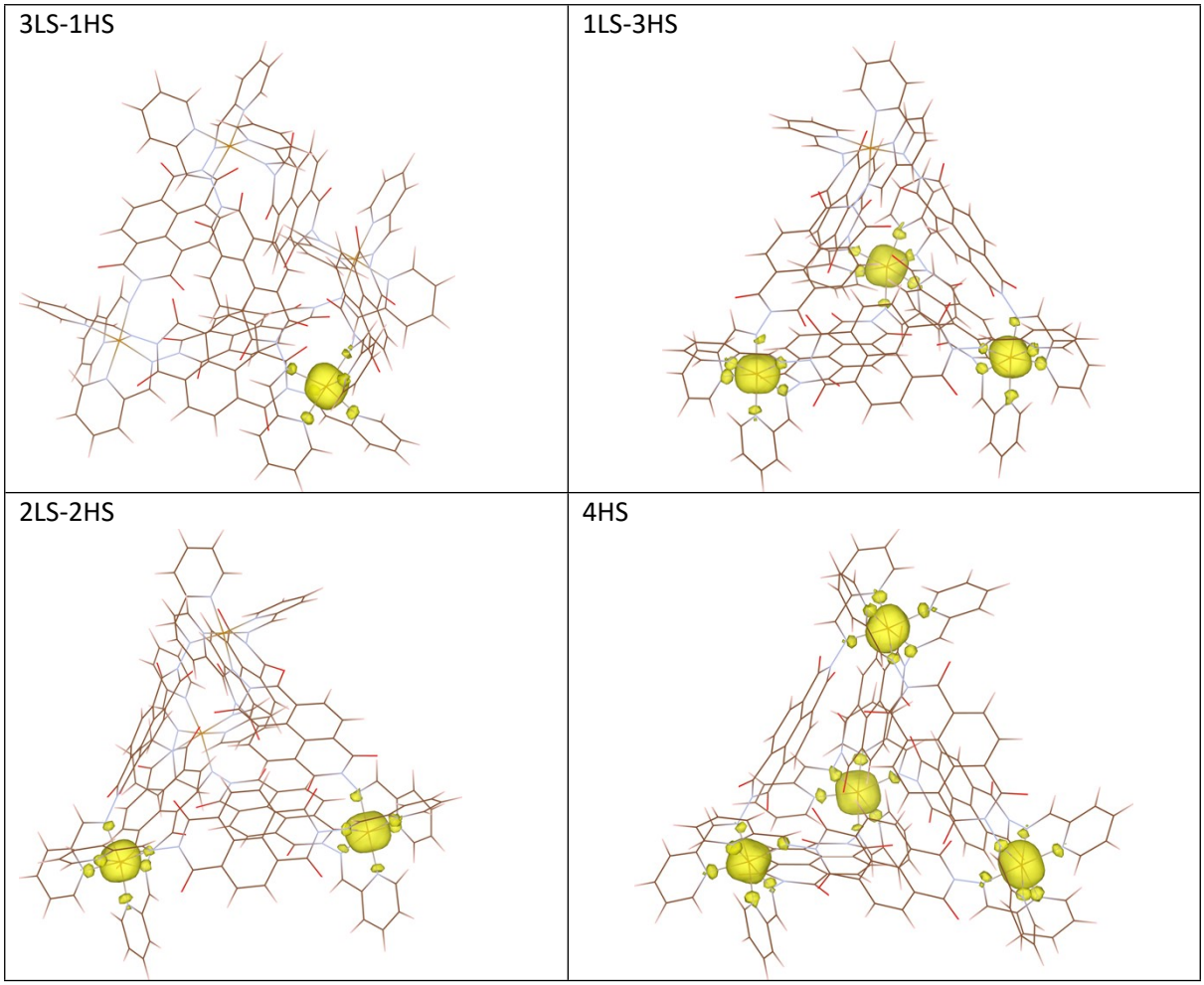

Fig. S11. B3LYP calculated spin density distribution for 3LS-1HS, 2LS-2HS, 1LS-3HS, and 4HS spin isomers of $[Fe^{II}_4L_6]^{8+}$ cage complex.

Table S7. Mononuclear iron(II) complexes with $\{FeN_6\}$ chromophore selected for DFT calibrations of the isomer shift[a]

	isomer shift (δ) (mm/s)	isomer shift (δ) recalculated for T = 4.2 K (mm/s)	Quadrupole splitting ΔE_Q *(mm/s)*
$[Fe(phen)_2(NCS)_2]$ (LS)	0.34	0.37	0.34
$[Fe(LN_4)(NCS)_2]$ (LS)	0.44	0.47	0.77
$[Fe(HC(3,5\text{-}Me_2pz)_3)_2]I_2$ (LS)	0.46	0.46	0.21
$[Fe(bipy)_3](ClO_4)_2$ (LS)	0.33	0.36	0.39
$[Fe(phen)_3](ClO_4)_2$ (LS)	0.34	0.37	0.23
$[Fe(terpy)_2]Cl_2$ (LS)	0.27	0.3	1
$[Fe(phen)_2(NCS)_2]$ (HS)	1.01	1.04	2.82
$[Fe(LN_4)(NCS)_2]$ (HS)	1.1	1.13	2.51
$[Fe(HC(3,5\text{-}Me_2pz)_3)_2]I_2$ (HS)	1.02	1.09	3.86
$[Fe(TMP)_2(NCS)_2]$ (HS)	1.07	1.11	3.27

[a] data taken from the publication: M. Pápai and G. Vankó, J. Chem. Theory Comput., 2013, 9, 5004–5020. LS = low-spin state, HS = high-spin state.

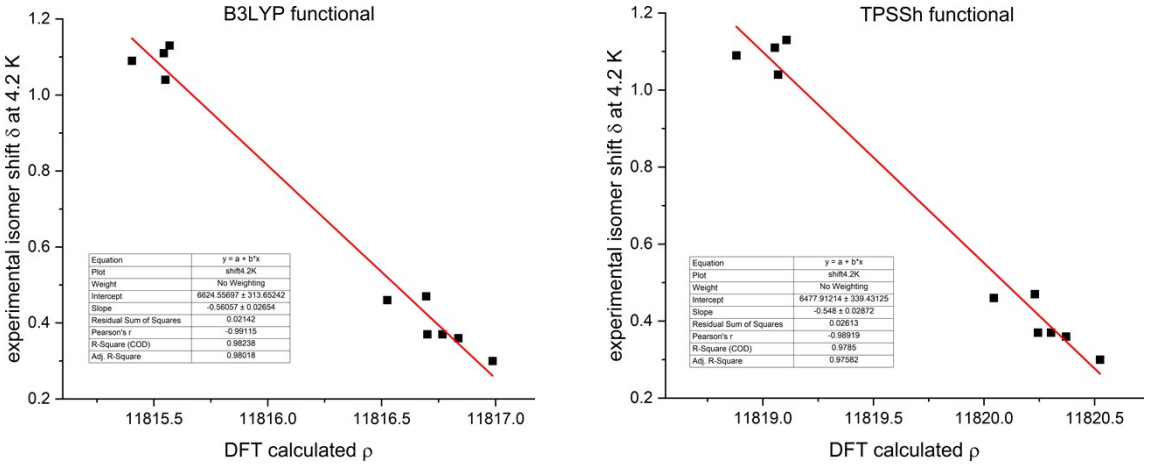

Fig. S12. Calibration of the isomer shift to DFT calculated electron density at the iron nucleus ρ for the mononuclear iron(II) complexes with $\{FeN_6\}$ chromophore.

Table S8. DFT calculated isomer shifts and quadrupole splitting for 4LS, 3LS-1HS, 2LS-2HS, 1LS-3HS, and 4HS spin isomers of $[Fe^{II}_4L_6]^{8+}$ cage complex.

	B3LYP	isomer shift (δ) calculated for T = 4.2K	$\lvert\Delta E_Q\rvert$		**TPSSh**	isomer shift (δ) calculated for T = 4.2K	$\lvert\Delta E_Q\rvert$
LS4	Fe1	**0.468**	**0.331**	**LS4**	Fe1	**0.425**	**0.388**
	Fe2	**0.468**	**0.337**		Fe2	**0.425**	**0.393**
	Fe3	**0.468**	**0.339**		Fe3	**0.425**	**0.394**
	Fe4	**0.468**	**0.334**		Fe4	**0.425**	**0.390**
LS3-HS1	Fe1	**1.063**	**3.394**	**LS3-HS1**	Fe1	**1.016**	**3.159**
	Fe2	**0.465**	**0.344**		Fe2	**0.423**	**0.399**
	Fe3	**0.465**	**0.329**		Fe3	**0.423**	**0.386**
	Fe4	**0.468**	**0.325**		Fe4	**0.425**	**0.382**
LS2-HS2	Fe1	**1.064**	**3.361**	**LS2-HS2**	Fe1	**1.016**	**3.126**
	Fe2	**1.062**	**3.483**		Fe2	**1.014**	**3.249**
	Fe3	**0.463**	**0.337**		Fe3	**0.420**	**0.393**
	Fe4	**0.465**	**0.319**		Fe4	**0.422**	**0.377**
LS1-HS3	Fe1	**0.463**	**0.325**	**LS1-HS3**	Fe1	**0.420**	**0.383**
	Fe2	**1.057**	**3.353**		Fe2	**1.010**	**3.117**
	Fe3	**1.062**	**3.441**		Fe3	**1.014**	**3.207**
	Fe4	**1.059**	**3.444**		Fe4	**1.011**	**3.209**
HS4	Fe1	**1.058**	**3.407**	**HS4**	Fe1	**1.011**	**3.172**
	Fe2	**1.057**	**3.415**		Fe2	**1.009**	**3.181**
	Fe3	**1.057**	**3.420**		Fe3	**1.009**	**3.185**
	Fe4	**1.058**	**3.400**		Fe4	**1.010**	**3.165**

The DFT calculations of the whole cage in the absence of anions showed that (i) the calculations can reproduce well the structure and the Mossbauer parameters of the cage (ii) the spin state change of each iron centre is independent of that of the other centres (as witnessed by the gradual and constant increase in energy when the spin state of a single iron centre is varied (iii) the B3LYP functional yielded the closes energy difference between the HS and LS states of the system, thus best reproducing the SCO properties of the cage.

However, in thermally induced SCO behaviour also occurs due to entropic effects, which we could not take into account in the whole cage calculations due to the size of the system, and we could not study the effect of anions either. In order to investigate these effects, we only considered one iron center with a simplified ligand structure, already used in our previous

work,[3] which maintained the essential features of the iron coordination sphere (see Fig S13). Ligand truncation in the calculation was furthermore necessary, as the overall cage structure is maintained by the coordination of one ligand with two iron centers. In the absence of the other iron centers, the whole system collapses during geometry optimization due to the non-covalent interactions between the far ends of the ligands. We considered four systems: an Fe^{2+} center with its ligands and models of the three cages including two anions. (cage **1**: BF_4^-, cage **2**: ClO_4^-. cage **3**: $CF_3SO_3^-$). Further calculations were performed on the anions, truncated ligands and full ligands in order to assess whether interaction between the anions and the full ligand is properly modelled by a truncated model of the ligand.

As the calculations of the whole cage showed that among the studied functionals B3LYP yielded the closest energetics to an SCO behaviour (smallest difference between LS and HS states) we performed geometry optimization was performed using both the B3LYP and the B3LYP* functionals in conjunction with the def2-SVP basis set.[4-6] We decided to use B3LYP* as well, because it is well-known that obtaining accurate energetics for spin state splittings of transition metal complexes is a notoriously difficult task due to the individual nature of the various systems, however, as a general rule the energetics can be tuned by varying the HF exchange included in hybrid functionals.[7] In accordance with general observations, B3LYP with 20% HF exchange favored the HS state of the complexes, while B3LYP* with 15% HS exchanged favored the LS state of the complexes. We experimented with tuning the functional and including about 18% HF exchange in the functional yielded nearly degenerate HS and LS states for the cages at 80 K. However, the trends observed with all functionals were the same and for this reason we stick to the discussion of the results of the commonly used B3LYP and B3LYP* functionals. RI density fitting approximation was integrated with the def2/J auxiliary basis set.[8] Relativistic effects and dispersion interactions were taken into account by including the zeroth-order relativistic approximation (ZORA)[9,10] and Grimme's Becke-Johnson damped dispersion correction (D3(BJ)).[11,12] Following the geometry optimization, all of the structures were characterized by harmonic vibration analysis at the same levels of theory, to ensure that the located stationary points are minima on the potential energy surface and to obtain the thermal correction for Gibbs Free Energy at 2 K, 80 K, 298.15 K, and 400 K respectively. Geometries were optimized in both the high spin (quintet) and low spin (singlet) states. In order to obtain more reliable energetics, single-point energy calculations were performed with the larger basis set def2-TZVP[4-6] and also included the treatment of scalar relativistic effects via

the ZORA[9,10] formalism, dispersion corrections (D3(BJ))[11,12] and CPCM solvation model (with acetone as solvent).

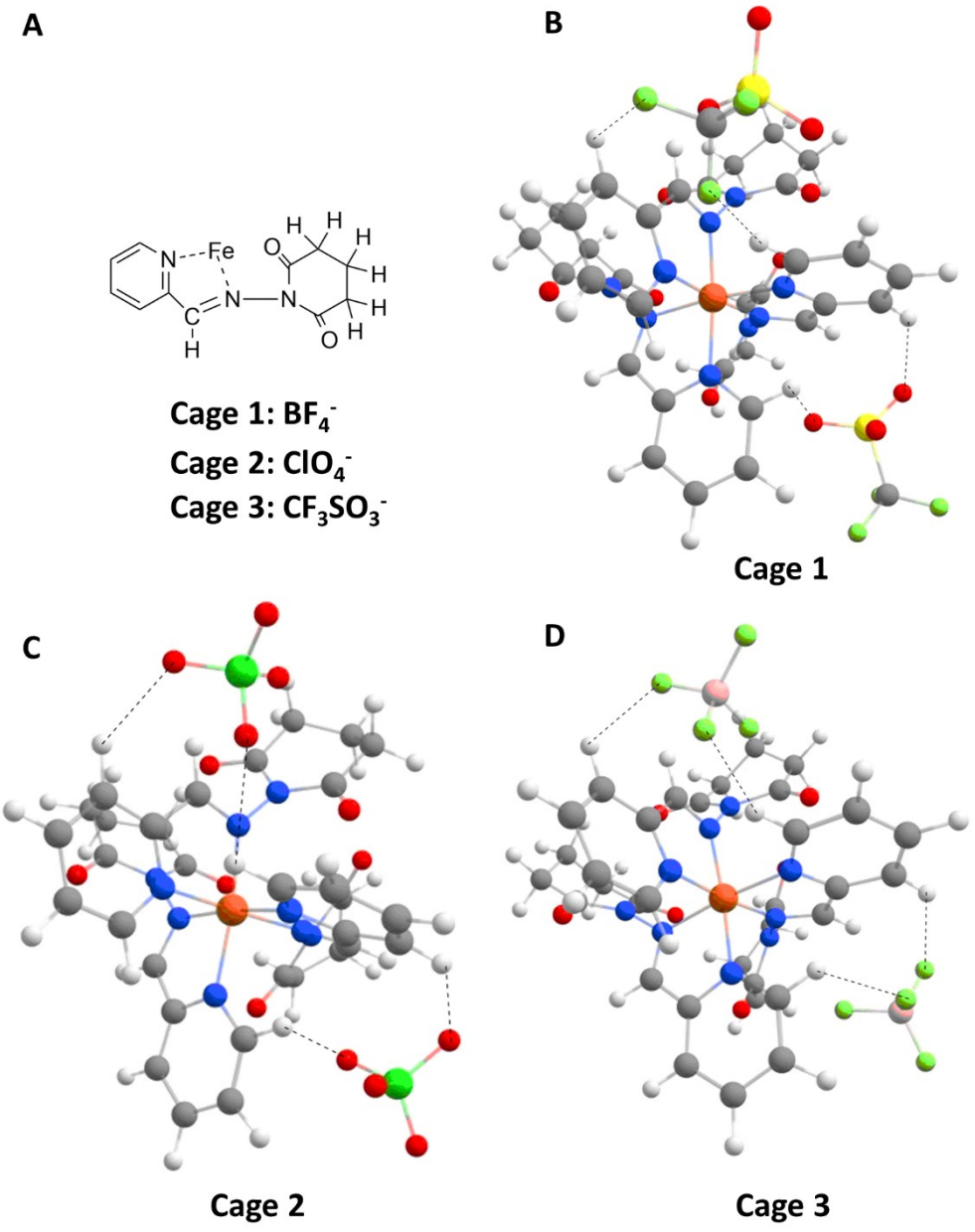

Fig. S13. **A**. Structure of the truncated ligand used in quantum chemical calculations. The model system included three ligands. **B-C-D**. Overall three-dimensional structure of the modeled systems in the LS state at the B3LYP/SVP level of theory and interaction of the anions (BF_4^-, ClO_4^- and $CF_3SO_3^-$, respectively) with the ligands.

Table S9. Variation of Fe-N bond lengths and Fe-X (X = Anion: X=B in the case of BF_4^-; X=Cl for ClO_4^-, and X=C for $CF_3SO_3^-$) bond distances for studied systems at the B3LYP/SVP level of theory

Bond Length	Model system	Fe-N	Fe-N	Fe-N	Fe-N	Fe-N	Fe-N	Fe-X1	Fe-X2
LS	Fe^{2+} Without Anions	2.012	2.002	1.986	2.019	1.999	2.000	-	-
	Cage 1	2.003	2.003	1.969	2.005	2.008	1.987	5.152	5.049
	Cage 2	1.995	1.995	1.979	1.994	2.004	1.996	5.350	5.558
	Cage 3	2.017	2.000	1.969	2.007	2.004	1.996	5.195	5.591
HS	Fe^{2+} Without Anions	2.180	2.207	2.178	2.223	2.183	2.214	-	-
	Cage 1	2.201	2.208	2.128	2.206	2.152	2.185	5.064	4.877
	Cage 2	2.196	2.196	2.138	2.178	2.152	2.204	5.332	5.128
	Cage 3	2.228	2.210	2.128	2.183	2.150	2.194	5.232	5.311

Table S10. Molecular orbital energies (in a.u.) of the iron d orbitals in the studied complexes at the B3LYP/SVP level of theory in the LS state.

Orbital	**Fe^{2+} without anions**[a]	Cage **1**	Cage **2**	Cage **3**
e_g	-0.207	-0.011	-0.017	-0.015
	-0.209	-0.014	-0.022	-0.019
Δ_o[b]	**0.125**	**0.114**	**0.116**	**0.101**
t_{2g}	-0.420	-0.223	-0.231	-0.226
	-0.424	-0.226	-0.232	-0.229
	-0.426	-0.230	-0.236	-0.233

[b] **Δ_o** has been calculated as the energy difference between the lowest lying e_g and the highest lying t_{2g} orbital

[a] the orbital energies calculated in the system without anions are lower than in the modelled cages, due to the positive charge of the system and lower number of electrons than protons. However, the orbital shapes and the Δ_o splitting is hardly affected.

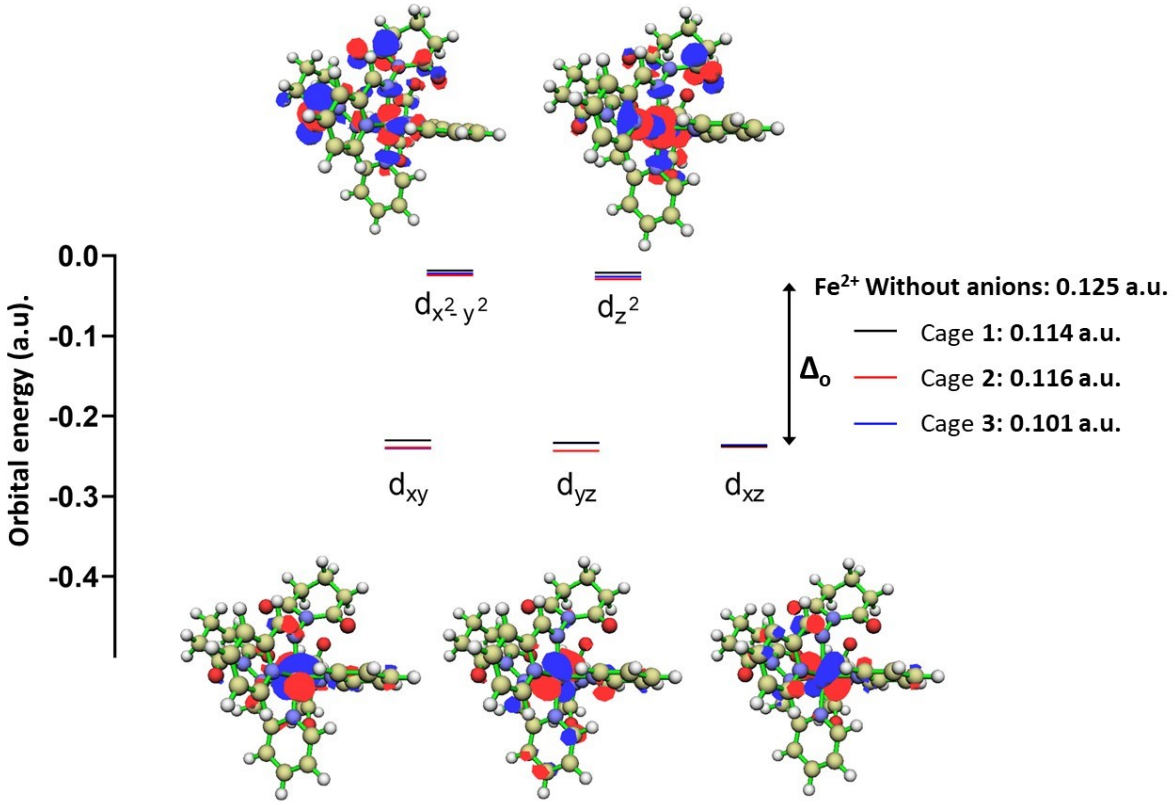

Fig. S14. Orbital energy splitting of the iron d orbitals in the model systems of the various cages.

Table S11 Mulliken charges of the Fe ion, Anions, and Ligands across the different cages and different spin states (with and without solvation) at the B3LYP/SV(P) level of theory.

Charges		With Implicit solvent model			Without Solvation		
		Fe	Sum of Anions	Sum of Ligands	Fe	Sum of Anions	Sum of Ligand
Fe^{2+} Without Anions	LS	0.70		1.30		0.70	1.30
	HS	0.93		1.07		0.93	1.07
Cage 1	LS	0.69	-1.48	0.79	0.70	-1.38	0.68
	HS	0.94	-1.47	0.53	0.94	-1.36	0.42
Cage 2	LS	0.69	-1.57	0.88	0.69	-1.50	0.80
	HS	0.93	-1.58	0.66	0.93	-1.49	0.56
Cage 3	LS	0.69	-1.56	0.87	0.70	-1.48	0.78
	HS	0.93	-1.56	0.63	0.93	-1.48	0.55

Table S12. Energy differences and Gibbs free energy differences at 80 K between the LS and HS states of the studied systems at various levels of theory in kcal/mol. A positive number shows that the HS state is more stable than the LS state.

Energy Difference (LS - HS) at 80 K						
Functional	**Basis set + solvent**	**Complex**	Electronic Energy (Without Dispersion)	Gibbs free energy (Without Dispersion)	Electronic Energy (With Dispersion)	Gibbs free energy (With Dispersion)
B3LYP	SVP	Fe^{2+}	2.3	5.4	-0.3	2.8
		cage1	0.1	3.1	-1.0	**2.0**[a]
		cage 2	-2.9	0.5	-4.4	**-0.9** [a]
		cage 3	0.2	2.1	-1.1	**2.1** [a]
	SVP + Acetone	Fe^{2+}	-0.4	2.7	-3.0	0.1
		cage1	0.7	3.7	-0.4	2.6
		cage 2	-1.8	1.7	-3.3	0.2
		cage 3	-1.2	1.9	-2.5	0.7
	TZVP	Fe^{2+}	2.7	5.8	0.2	3.2
		cage1	-0.3	2.7	-1.4	1.6
		cage 2	-1.2	2.3	-2.7	0.8
		cage 3	0.5	3.6	-0.8	2.4
B3LYP *	SVP	Fe^{2+}	-5.4	-2.2	-8.1	-4.9
		cage1	-7.1	-4.0	-8.3	-5.3
		cage 2	-1.5	2.0	-11.5	-8.1
		cage 3	-7.1	-4.1	-8.3	-5.2
	SVP + Acetone	Fe^{2+}	-8.2	-5.0	-10.9	-7.7
		cage1	-6.8	-3.7	-8.0	-4.9
		cage 2	-0.4	3.1	-10.6	-7.2
		cage 3	-8.8	-5.7	-9.9	-6.9
	TZVP	Fe^{2+}	-4.7	-1.5	-7.4	-4.2
		cage1	-7.4	-4.3	-8.6	-5.5
		cage 2	0.3	3.7	-9.9	-6.5
		cage 3	-6.7	-3.7	-7.9	-4.8

[a] **data quoted in main manuscript.**

Table S13. Interaction energies and interaction Gibbs free energies (at 80 K) in kcal/mol between the iron-complex with its ligands and the anions at various level of theory based on the reaction: Fe^{2+}-ligands + 2 $anions^-$ → [[Fe^{2+}-ligands]2$anions^-$].

Functional	Basis set	Complex	Interaction Energy (Without Dispersion)		Interaction Gibbs free Energy (Without Dispersion)		Interaction Energy (With Dispersion)		Interaction Gibbs free Energy (With Dispersion)	
			HS	LS	HS	LS	HS	LS	HS	LS
B3LYP	SVP	cage1	-222.7	-224.9	-213.8	-216.0	-240.5	-241.3	-231.6	-232.4
		cage 2	-205.7	-210.9	-197.3	-202.2	-228.3	-232.5	-219.9	-223.7
		cage 3	-204.2	-206.4	-388.9	-392.3	-229.8	-230.6	-220.7	-221.5
	SVP + Acetone[a]	cage1	-16.8	-15.7	-7.8	-6.8	-34.6	-32.0	-25.7	-23.2
		cage 2	-9.9	-11.4	-1.6	-2.6	-32.6	-32.9	-24.2	-24.1
		cage 3	-10.2	-11.1	-1.2	-2.0	-35.8	-35.3	-26.7	-26.2
	TZVP	cage1	-179.3	-182.3	-170.3	-173.4	-197.1	-198.7	**-188.2**[b]	**-189.8**[b]
		cage 2	-179.6	-183.5	-171.2	-174.7	-202.2	-205.0	**-193.9**[b]	**-196.3**[b]
		cage 3	-171.9	-174.1	-162.8	-165.0	-197.4	-198.3	**-188.4**[b]	**-189.2**[b]
B3LYP*	SVP	cage1	-226.4	-228.1	-217.4	-219.2	-244.2	-244.5	-235.2	-235.6
		cage 2	-209.0	-213.9	-200.5	-205.1	-232.0	-233.6	-223.6	-226.8
		cage 3	-207.4	-209.1	-198.2	-200.1	-233.3	-233.6	-224.2	-224.5
	SVP + Acetone[a]	cage1	-19.1	-17.7	-10.1	-8.8	-36.9	-34.0	-28.0	-25.2
		cage 2	-11.9	-13.1	-3.5	-4.4	-35.0	-34.8	-26.5	-26.0
		cage 3	-12.2	-12.8	-3.0	-3.7	-38.2	-37.2	-29.0	-28.1
	TZVP	cage1	-180.9	-183.6	-171.9	-174.7	-198.7	-199.9	-189.7	-191.1
		cage 2	-181.0	-185.1	-172.6	-176.3	-204.1	-206.7	-195.7	-198.0
		cage 3	-173.1	-175.2	-163.9	-166.1	-199.1	-199.6	-189.9	-190.6

[a] numbers obtained with the inclusion of the solvent model are significantly smaller than those calculated in vacuo due to the fact that in vacuo when we bring three ions from infinitely far away to close contact there is a huge stabilization due to the favorable Coulombic interactions, while in solvent the ions are stabilized to some extent, which will reduce the calculated energy/Gibbs free energy gain of bringing the ions close to each other

[b] Values quoted in the main manuscript

References

(1) F. Neese, *Wiley Interdiscip. Rev. Comput. Mol. Sci.* **2012**, *2*, 73–78.

(2) F. Neese, Software update: the ORCA program system, version 4.0. *WIREs Comput. Mol. Sci.* **2018**, *8*, 1327.

(3) W. Li, C. Liu, J. Kfoury, J. Oláh, K. Robeyns, M. L. Singleton, S. Demeshko, F. Meyer, Y. Garcia. *Chem. Commun.* **2022**, 58, 11653-11656.

(4) A. D. Becke, *Phys. Rev. A* **1988**, *38*, 3098–3100.

(5) J. P. Perdew, *Phys. Rev. B* **1986**, *33*, 8822–8824.

(6) F. Weigend, R. Ahlrichs, *Phys. Chem. Chem. Phys.* **2005**, *7*, 3297.

(7) J. N. Harvey, *Annu. Rep. Prog. Chem., Sect. C*, 2006, 102, 203–226.

(8) F. Weigend, *Phys. Chem. Chem. Phys.* **2006**, *8*, 1057.

(9) C. Van Wüllen, *J. Chem. Phys.* **1998**, *109*, 392–399.

(10) D. A. Pantazis, X. Chen, C. R. Landis, F. Neese, *J. Chem. Theory Comput*. **2008**, *4*, 908–919.

(11) E. R. Johnson, A. D. Becke, A post-Hartree-Fock model of intermolecular interactions: Inclusion of higher-order corrections. *J. Chem. Phys.* **2006**, *124*, 174104.

(12) S. Grimme, S. Ehrlich, L. Goerigk, *J. Comput. Chem.* **2011**, *32*, 1456–1465.